ISME

H. Aminfar*
Associate Professor

M. R. Haghgoo†
M.Sc. Student

Modeling of Upward Subcooled Flow Boiling of Refrigerant-113 in a Vertical Annulus

In this paper, a modified two-fluid model has been adopted to simulate the process of upward vertical subcooled flow boiling of refrigerant R-113 in a vertical annular channel at low pressure. The modified model considers temperature dependent properties and saturation temperature variation and was validated against a number of published low-pressure subcooled boiling experiments. The results show good agreement with experimental data including radial profiles of void fraction, phase velocities and liquid temperature. A sinusoidal axial distribution of wall heat flux was applied as well as constant wall heat flux. Results show that by increasing the wall heat flux, the bubble boundary layer will become thicker and the profiles of axial liquid velocity will gradually depart from those of single-phase flow.

Keywords: Two-fluid model, Refrigerant-113, Saturation temperature variation, Subcooled boiling flow

1 Introduction

Subcooled flow boiling can be found in many practical applications, such as heat exchangers, steam generators, refrigeration systems and it is especially important in water-cooled nuclear power reactors, where the presence of vapor bubbles in the core influences the reactor behavior at operating and accident conditions. At high heat-flux densities, vaporization may occur at the heated surface despite the fact that the mean temperature of the cooling liquid has not yet reached the saturation point. This phenomenon is called "subcooled boiling," which is caused by a thermodynamic nonequilibrium in the liquid. There is a superheated liquid in the boundary layer near the heated wall, while the bulk temperature is still fairly subcooled.

In subcooled boiling flow in a vertical channel, vapor distribution not only is uneven over the channel cross section but also evolves along the flow, as both the void fraction and the width of the two-phase layer near the heated surface gradually increase. This non-uniform distribution of vapor enormously influences hydrodynamic and thermal processes, including heat transfer. Although a significant amount of literature deals with the cross-sectional distribution of the gas phase in adiabatic bubbly flow, investigations of analogous phenomena in boiling flow have been much less common.

Among multidimensional theoretical analysis of subcooled boiling flow, the most widely used approach so far appears to be two-fluid modeling [1]. This model treats the general case of modeling each phase or component as a separate fluid with its own set of governing

* Associate Professor, Mechanical Engineering Department, University of Tabriz
† Corresponding Author, M.Sc. Student, Mechanical Engineering Department, University of Tabriz
haghgoo.reza87@ms.tabrizu.ac.ir

equations which were coupled with interfacial mass, momentum and energy transfer, respectively. In general each phase has its own velocity, temperature and pressure.
Kurul and Podowski [2] proposed a modified two-fluid model in which the total heat flux split into three different modes of heat transfer (i.e. single phase convection heat flux, quenching heat flux and wall evaporation heat flux). Mimouni et al. [3] and Krepper et al. [4] have recently applied the aforementioned model to simulate boiling flow .Lai and Farouk [5], in their numerical investigation, prescribed a 1 mm bubble diameter in the flow field to perform two dimensional numerical simulations while Kurul and Podowski [2] and Anglart and Nylund [6] modelled the bubble diameter as a linear function of local liquid subcooling with its maximum value located in the near-wall cell.

The two-fluid model has been applied either to boiling of refrigerant at low pressure or to boiling of water at high pressure. However, numerical studies of Hari and Hassan [7], Koncar et al. [8] and Hainoun et al. [9] showed that the extrapolation of models developed for water at high pressure condition to low pressure usually leads to erroneous results. Namely, although the generic features of the two-fluid model are the same, many closure relations describing mass, momentum and energy exchange at the gas–liquid interface do not apply to both high-pressure and low-pressure conditions. Janssens-Maenhout et al. [10] proposed a multidimensional two-fluid model for subcooled boiling flow of water at low pressure. Lee et al. [11] have also successfully applied their model to the simulation of their own experimental results of subcooled boiling flow of water at low pressure.

Legendre et al. [12] presented a promising approach for modeling of boiling based on local instantaneous description of the flow field. However, due to the complex structure of the interface in subcooled nucleate boiling, this approach is still computationally too demanding for simulating boiling systems over a significant portion of a channel. Keljenak et al. [13] have recently successfully applied Langrangian bubble-tracking method to simulate the trajectories and interactions of individual bubbles for simulation of boiling flows. However, this method is mostly limited to diluted bubbly flows and is computationally more time consuming than Eulerian methods.

St Pierre and Bankoff [14] experimentally investigated subcooled boiling in a vertical rectangular channel with heated walls at pressures ranging from 1.4 to 5.5 bar. They measured transverse void fractions over the channel cross-section at different elevations. Anglart and Nylund [6] measured radial void fraction profiles in an annular test section with a heated inner rod. Sekoguchi et al. [15] experimentally determined radial void fraction profiles in cylindrical tubes with heated walls at pressures 2, 4 and 8 atm. Bartel [16] also experimentally obtained radial profiles of flow parameters at different axial locations in a vertical annulus with a heated inner rod, at near atmospheric pressure.

Model improvements are usually concentrated on two phase wall function, wall heat flux partition, bubble departure diameter etc., whereas few investigations have been done on the temperature dependent properties of fluid in subcooled boiling flow and saturation temperature variation along the heated channel [17].

As the main purpose of the current study is to investigate the multidimensional aspects of subcooled boiling, experiments in which the non-homogeneous cross-sectional distribution of flow parameter were determined (such as void fraction or heat transfer coefficient, related to the cross-sectional average temperature) are not considered here. Accordingly the primer focus of the present study is on the radial profiles of void fraction, phase velocities and liquid temperature.

In the present work, the general-purpose computational fluid dynamics code CFX-12 was used as a framework for solving the generic two-fluid model with additional relevant closure relations, and user defined CEL (CFX Expression Language) functions were acted as an important tool to implement the definition of temperature dependent properties.

2 Governing equations

As derived in the two-fluid model by Ishii and Mishima [18] the mass balance equation for a phase in steady state is given as:

$$\nabla.(\alpha_k \rho_k \mathbf{u}_k) = \Gamma_k \tag{1}$$

where Γ_k is the rate of a phase change for the k phase and α is the phase fraction.
The momentum equations in steady state are given as follows.

$$\begin{aligned}\nabla.(\alpha_k \rho_k \mathbf{u}_k u_k) = -\nabla(\alpha_k p) + \nabla.[\alpha_k(\bar{\bar{\tau}}_k + \tau_k^T)] + \alpha_k \rho_k \mathbf{g} \\ + u_{ki}\Gamma_k + F_{ik} - \nabla\alpha_k.\tau_{ki} + p\nabla\alpha_k\end{aligned} \tag{2}$$

where $\bar{\bar{\tau}}_k$ and τ_k^T are the molecular stress tensor and the turbulent stress tensor, respectively. F_{ik} denotes the term of an interfacial momentum transfer including the interfacial drag force, the wall lubrication force, the lift force and the turbulent dispersion force.

Energy equations are expressed as a form of the enthalpy (H_k) transport of each phase.

$$\nabla.(\alpha_k \rho_k H_k \mathbf{u}_k) = -\nabla.[\alpha_k(\bar{\mathrm{q}}_k + \mathrm{q}_k^T)] + \alpha_k \frac{D_k p}{Dt} + H_{ki}\Gamma_k + q''_{ki} a_i \tag{3}$$

here, q_k is a diffusive flux by a conduction and the superscript 'T' means the enhanced flux by a turbulence. q''_{ki} is the interfacial heat flux between two phases, defined as $h_i(T_s - T_k)$, and a_i is the interfacial area density. From the energy equation for a boiling flow, the phase changes due to a wall boiling (Γ_w) and a bulk condensation (Γ_{ig}) can be estimated as follows.

$$\Gamma_w = \frac{q_e}{H_{sg} - H_l} \tag{4}$$

$$\Gamma_{ig} = -\frac{h_i a_i (T_s - T_l) + h_i a_i (T_s - T_g)}{H_g - H_{sl}} \tag{5}$$

here, q_e is the amount of evaporative heat transfer from the heated wall. From Eqs. (4) and (5), the rate of a phase change can be determined as follows.

$$\Gamma_g = -\Gamma_l = \Gamma_w + \Gamma_{ig} \tag{6}$$

Boussinesq approximation was used in the momentum equation, so that the gravitational acceleration was modified as given in Eq. (7). This approximation makes it possible to utilize a constant density of each phase.

$$-\frac{1}{\rho}\nabla p + \mathbf{g} \cong -\frac{1}{\rho_0}\nabla p + \mathbf{g}(1 + \beta\Delta T) \tag{7}$$

Liquid turbulence is estimated by the Standard $k-\varepsilon$ model which is a kind of Reynolds-Averaged Navier-Stokes (RANS) equation. In a two-phase flow with a phase change, transport equations for the turbulent kinetic energy, k, and the dissipation, ε, are formulated as follows.

$$\nabla.(\alpha_l \rho_l \mathbf{u}_l k) = \nabla.[\alpha_l(\mu + \frac{\mu_t}{\sigma_k})\nabla k] + \alpha_l P - \alpha_l \rho_l \varepsilon \tag{8}$$

$$\nabla.(\alpha_l \rho_l \mathbf{u}_l \varepsilon) = \nabla.[\alpha_l(\mu + \frac{\mu_t}{\sigma_\varepsilon})\nabla\varepsilon] + \frac{\alpha_l \varepsilon}{k}(C_{\varepsilon 1} P - C_{\varepsilon 2}\rho_l \varepsilon) \tag{9}$$

here, P is the production rate of a turbulent kinetic energy. From the turbulent kinetic energy and dissipation, the turbulent diffusive flux of momentum or energy can be calculated with a turbulent viscosity. The coefficients used in this study are:

$\sigma_k = 1.0, \sigma_\varepsilon = 1.4, C_{\varepsilon 1} = 1.44, C_{\varepsilon 2} = 1.92$

Interfacial transfer of momentum, heat and mass is directly dependent on the contact surface area between the two phases known as the interfacial area density.

The Particle model for interfacial transfer between two phases assumes that one of the phases is continuous (liquid phase) and the other is dispersed (gas phase). The interfacial area density is then calculated by assuming that dispersed phase is present as spherical particles of Mean Diameter d_b.

$$a_i = \frac{6\alpha_g}{d_b} \tag{10}$$

$$\alpha_g = \begin{cases} max(r_b, r_{min}) & , \ if(r_b < r_{max}) \\ max\left(\frac{1-r_b}{1-r_{max}} r_{max}, r_{min}\right), & if(r_b > r_{max}) \end{cases} \tag{11}$$

here $r_b = \frac{N_b V_b}{V}$ where N_b and V_b are number of the bubbles and volume of each bubble in the computational cell respectively and V is the volume of computational cell. r_{max} and r_{min} take values of 0.8 and 10^{-7}, respectively [19].

3 Constitutive relations

3.1 Wall boiling model

In the subcooled boiling flow, the amount of vapor generation can be computed using a wall heat flux partitioning model. The mechanisms of a heat transfer from a wall consist of the single-phase convection (q_c), surface quenching (q_Q) and evaporative heat transfer (q_e) as follows.

$$\begin{gathered} q_w = q_c + q_Q + q_e \\ = S_t \rho_l C_{pl} A_{1\emptyset} u_l (T_w - T_l) + 2f(\tau_Q \lambda_l \rho_l C_{pl}/\pi)^{0.5} A_{bub}(T_w - T_l) \\ + N_a f \pi d_{bw}^3 \rho_g H_{lg}/6 \end{gathered} \tag{12}$$

where S_t is the local Stanton number, f is the bubble nucleation frequency, T_w is the wall temperature, T_l and u_l are the local liquid temperature and the velocity in the near-wall computational cell, respectively. The quenching period τ_Q between the departure of a bubble and the beginning of the growth of a subsequent one is defined as τ_Q=0.8/ f. The A_{bub} is the area fraction influenced by the nucleating bubbles and is usually formulated as A_{bub}=min[1, $\pi N_a d_{bw}^2$], where N_a is active nucleation sites density and d_{bw}^2 is the bubble departure diameter. whereas the remaining fraction $A_{1\phi} = 1 - A_{bub}$ is influenced only by the single-phase convection.

The model for wall nucleation site density adopted in the wall heat flux partitioning model is that of Lemmert and Chawla [20].

$$N_a = (185(T_w - T_l))^{1.805} \tag{13}$$

Cole correlation (1960, cited by Ivey [21]) was adopted to compute the bubble nucleation frequency f.

$$f = \sqrt{4\mathrm{g}(\rho_l - \rho_\mathrm{g})/(3d_{bw}\rho_l)} \tag{14}$$

for the bubble departure diameter, a Tolubinsky and Kostanchuk correlation [22] was applied.

$$d_{bw} = min\left(0.6[mm]exp(-\frac{\Delta T_{sub}}{45[K]}),1.4[mm]\right) \tag{15}$$

3.2 Thermal phase change model

In subcooled boiling flow, the inter-phase heat and mass transfer between the two phases are described by the bubble evaporation on the heated wall (Section 3.1) and the bubble condensation in bulk flow. After departure from the heated wall, the vapor bubbles are supposed to be surrounded by subcooled liquid and become condensed. The process of phase change induced by inter-phase heat transfer in subcooled boiling flow can be simulated by thermal phase change model. The rate of inter-phase heat transfer $Q_{l\mathrm{g}}$ across the phase boundary per unit time per unit volume is:

$$Q_{l\mathrm{g}} = h_i a_i (T_\mathrm{g} - T_l) \tag{16}$$

where, h_i is the inter-phase heat transfer coefficient, defined as $h_i = Nu_b\lambda_l/d_b$ and a_i is the interfacial area density described previously. For a particle in a moving incompressible Newtonian fluid, the bubble Nusselt number Nu_b can be calculated from the Ranz-Marshall correlation [23]:

$$Nu_b = 2 + 0.6Re_b^{0.5}Pr_l^{1/3} \tag{17}$$

In Eq. (17), Re_b is the bubble Reynolds and Pr_l is the surrounding liquid Prandtl Number.

3.3 Inter-phase momentum transfer

The interfacial transfer of momentum is modeled with the interfacial forces, which includes drag force $\boldsymbol{F}_D$, lift force $\boldsymbol{F}_L$, turbulent dispersion force $\boldsymbol{F}_{TD}$ and wall lubrication force $\boldsymbol{F}_W$ [19].
The interfacial drag force is calculated as:

$$\boldsymbol{F}_D = \frac{3C_D}{4d_b}\alpha_\mathrm{g}\rho_l\left|\mathbf{u}_\mathrm{g} - \mathbf{u}_l\right|(\mathbf{u}_\mathrm{g} - \mathbf{u}_l) \tag{18}$$

the interfacial drag coefficient in Eq. (18), C_D, is based on Ishii and Zuber's model [24].

- Spherical Regime: $$C_{D1} = \frac{24}{Re_b}(1 + 0.1Re_b^{0.75}) \tag{19}$$

- Spherical Cap Regime: (20)

- Distorted regime: $$C_{D3} = \frac{(1 + 17.67(1-\alpha_\mathrm{g})^{1.3})}{18.67(1-\alpha_\mathrm{g})^{1.5}}C_{D\infty} \tag{21}$$

$$C_D = \begin{cases} C_{D1} & ,C_{D1} > C_{D3} \\ min(C_{D2}, C_{D3}) & ,C_{D1} < C_{D3} \end{cases} \tag{22}$$

in Eqs. (19) and (21) the bubble Reynolds number, Re_b ,and $C_{D\infty}$ are defined respectively as:

$$Re_b = \frac{\rho_l |u_g - u_l| d_b}{\mu_m} \quad , \quad \frac{\mu_m}{\mu_l} = \frac{1}{1-\alpha_g} \quad , \quad C_{D\infty} = \frac{2}{3}(Eo)^{0.5} \, , Eo = \frac{g\Delta\rho d_b^2}{\sigma}$$

where Eo is the Eotvos number which measures the ratio between gravitational and surface tension forces. Here, $\Delta\rho$ and σ are gravitational acceleration, density difference between the phases and surface tension coefficient.

To predict a non homogeneous radial void fraction distribution, the non-drag forces, which act perpendicularly to the flow direction, also need to be modeled. The lift force on the liquid phase can be calculated as:

$$\boldsymbol{F}_L = C_L \alpha_g \rho_l (\mathbf{u}_g - \mathbf{u}_l) \times (\nabla \times \mathbf{u}_l) \tag{23}$$

Using the Tomiyama model [25], the lift force coefficient can be calculated as:

$$C_L = \begin{cases} min\left[0.288\, tanh\left(0.121 Re_b, f(Eo')\right)\right] & , Eo' \le 4 \\ f(Eo') & , 4 < Eo' \le 10 \\ -0.27 & , Eo' > 10 \end{cases} \tag{24}$$

where

$$f(Eo') = 0.00105 Eo'^3 - 0.0159 Eo'^2 - 0.0204 Eo' + 0.474 \tag{25}$$

here Eo' is modified Eotvos number (Eo) defined as follow.

$$Eo' = \frac{g(\rho_l - \rho_g) d_H^2}{\sigma} \quad , \quad d_H = d_b (1 + 0.163\, Eo^{0.757})^{1/3}$$

The effect of diffusion of the vapour phase, caused by liquid phase turbulence, is described with the turbulent dispersion force:

$$\boldsymbol{F}_{TD} = C_{TD} \frac{3 C_D \mu_l^{eff}}{4 d_b \sigma_t} \left(\frac{\nabla \alpha_g}{\alpha_g} - \frac{\nabla \alpha_l}{\alpha_l} \right) \tag{26}$$

where μ_l^{eff} is total dynamic viscosity of liquid and σ_t is the turbulent Schmidt number for the liquid phase with the value 0.9. C_{TD} denotes the turbulent dispersion coefficient which has a default value of 1.0.

The contribution of the wall lubrication force in the subcooled boiling flow is probably the most difficult to evaluate, as it acts only on those near-wall bubbles which have already abandoned the wall. In the case, when there is some liquid flow between the bubble and the wall, the wall lubrication force acts in lateral direction away from the wall and prevents the accumulation of bubbles on the wall. The model of Antal et al. [26] has been used for wall lubrication force:

$$\boldsymbol{F}_W = -\alpha_g \rho_l \frac{\left(\mathbf{u}_g - \mathbf{u}_l\right)^2}{d_b} max\left(C_1 + C_2 \frac{d_b}{y_w}, 0\right) \mathbf{n} \tag{27}$$

where y_w denotes the distance to the nearest wall, $\mathbf{n}$ is the unit normal pointing away from the wall and C_1 and C_2 are -0.01 and 0.05, respectively. The wall lubrication force approaches infinity as the wall distance approaches zero ensuring zero void fraction on the wall.

4 Numerical method, validation and boundary conditions

The set of coupled differential equations has been discretized by a control volume technique. In calculating a convection term, the upwind scheme has been applied for a numerical stability of the solution and the Rhie and Chow option [27] has been used for discretization of the mass flows to lead to proper pressure-velocity coupling. Here the test section has been modeled as a 45° sector of the annular channel and its length is 3.66 m with a 2.75 m long

upper heated part. The inner and outer diameters of the test section are 15.78 and 38.02 mm, respectively. Fig. 1 shows the predicted distributions of void fraction and liquid temperature in the aforementioned channel. The calculation of transversal profiles of void fraction, phase velocities and liquid temperature has been performed at a single axial location located 2.059 m downstream from the beginning of the heated section, known as measurement plane (M.P.). The pressure at this plane has been reported to be 0.269 MPa. [28].

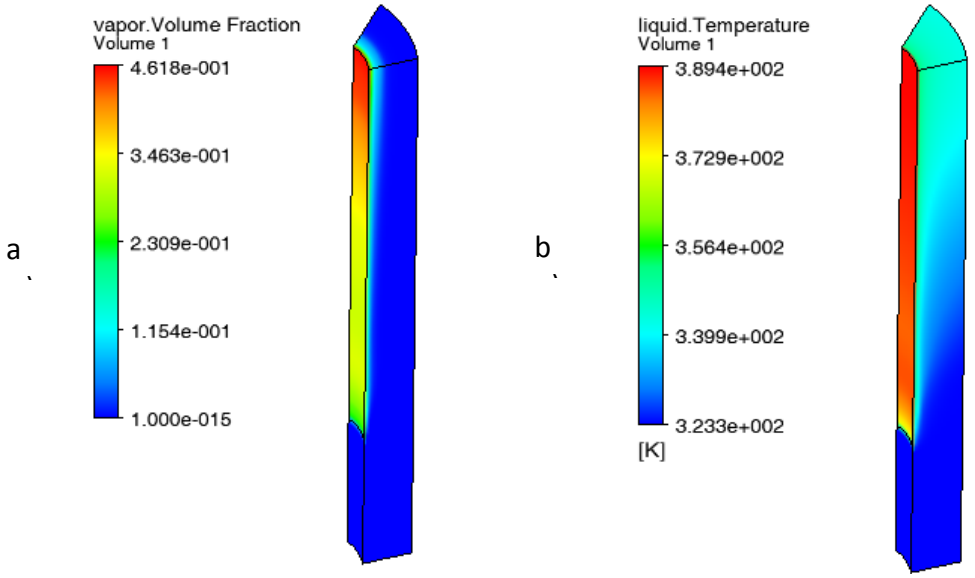

Figure 1 Predicted distributions of a) void fraction and b) liquid temperature, in the annular channel for mass flux, inlet temperature and wall heat flux equal to 784 (Kg/m^{2}s) , 323.35 (K) and 116 (kW/m^2), respectively.

Several different grid distributions have been examined to ensure that the estimated results are grid independent. As shown in Fig. 2 increasing the grid numbers does not change significantly the longitudinal and axial void fraction at heated wall and measurement plane (M.P.), respectively. Therefore the computational domain has been divided into 20×6×100 uniform grids in radial, circumferential and axial directions, respectively.

Numerical results are validated against published experimental data on subcooled boiling flow of Refrigerant-113 done by Kang and Roy [28]. In order to show the application of the modified model, the numerical results of Koncar et al. [29] are compared and analyzed with the present work, too. Hereinafter, the prefix ‘‘Calcu” means the predicted results using the modified model, while the prefix ‘‘Koncar” represents the calculated data in Ref. [29].

The steady-state computational model has been used. For the liquid phase a no-slip and for the gaseous phase a free slip boundary condition has been applied. Constant heat flux boundary condition as well as sinusoidal axial distribution of wall heat flux has been adopted on the heated wall and pressure boundary condition has been applied at the outlet. Uniform velocity and temperature profiles have been set at the inlet of the annulus channel. Besides, the two sections connected with heated wall along the annular channel have been defined as symmetry planes. A k-ε turbulence model is employed for the continuous phase while the dispersed vapor phase remains laminar. The Sato’s eddy viscosity model [30] is adopted to compute the bubble-induced turbulence viscosity.

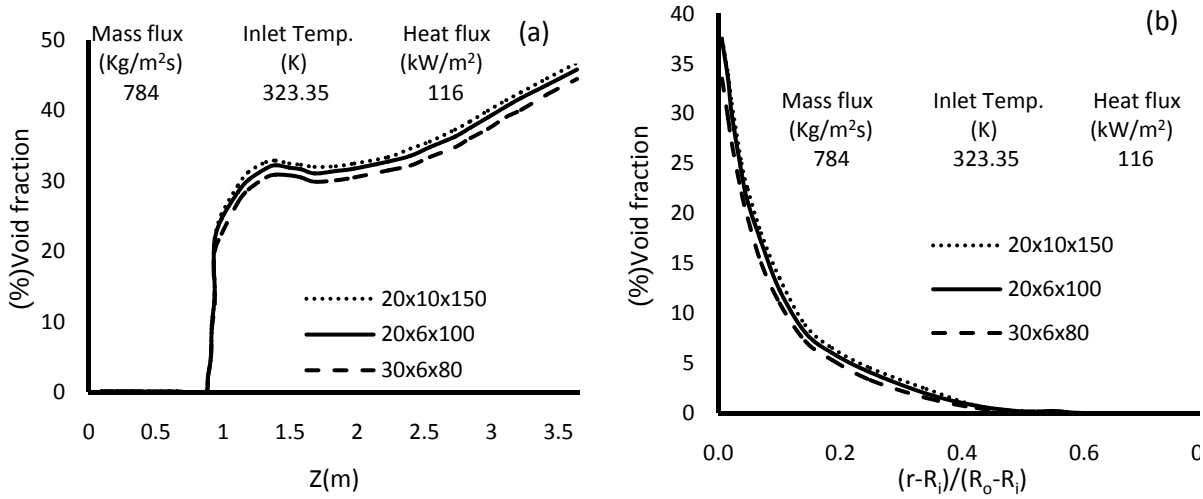

Figure 2 Grid influence on (a) longitudinal void fraction at heated wall (b) radial void fraction at M.P.

5 Results and Discussion

5.1.1 Influence of temperature dependent properties

Table 1 shows the physical properties of liquid refrigerant 113 (at 0.269 MPa) at different liquid subcoolings [17]. When liquid subcooling varies from 0 to 40 K, density, thermal conductivity, viscosity and specific heat at constant pressure increase by 6.7%, 13.5%, 57.1%, −4.7%, respectively. Therefore, temperature dependent properties should be given extra considerations in order to accurately simulate subcooled boiling flow. Fig. 3(a) and (b) present the influence of temperature dependent properties on the predicted void fraction profile and liquid temperature profile at the measurement plane. The ‘‘Constant properties” denotes the saturated liquid properties adopted, while ‘‘Variable properties” means that the liquid properties vary with liquid subcooling. In the whole, temperature dependent properties have little influence on the predictions of local flow characteristics in subcooled boiling flow.

Table 1 Physical properties of liquid refrigerant-113 (at 0.269 MPa)

Subcooling (K)	Density (kg/m^3)	Therm. Cond. (mW/m K)	Viscosity (μPa/s)	C_p (J/kg K)
0	1423	57.37	340.8	978.6
10	1450	59.26	379.3	966.0
20	1476	61.18	423.5	954.2
30	1501	63.13	474.9	943.2
40	1526	65.12	535.5	932.8

5.1.2 Influence of saturation temperature

The saturation temperature may vary evidently along the heated channel (for about 5 K in a 3 m long vertical channel). Three models of saturation temperature has been used, including two constant saturation temperatures corresponding to the inlet and the outlet pressures of heated channel, and a linear saturation temperature correlation between each other. Fig. 4(a) and (b) present the influence of the saturation temperatures on the predicted void fraction profile and liquid temperature profile at the measurement plane. When the saturation temperature drops, the evaporation heat flux will increase and the remainder heat flux used for

heating liquid will decrease. Subsequently, more vapor bubbles will be generated and the liquid temperature at the near-wall region will be lower [17].

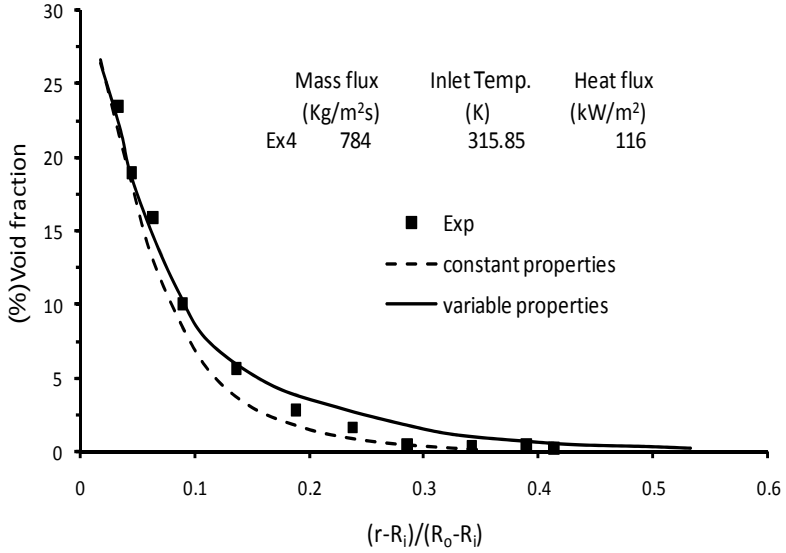

(a) Predicted void fraction profile at M.P.

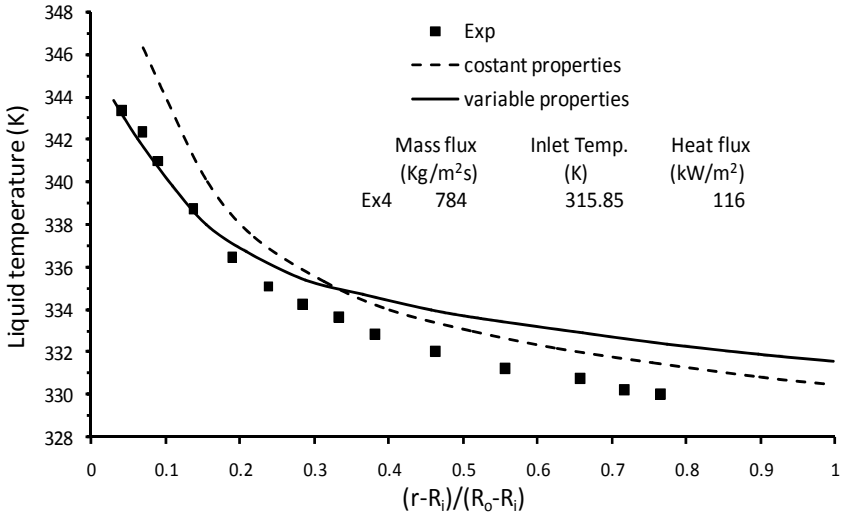

(b) Predicted Liquid temperature profile at M.P.

Figure 3 Influence of temperature dependent properties.

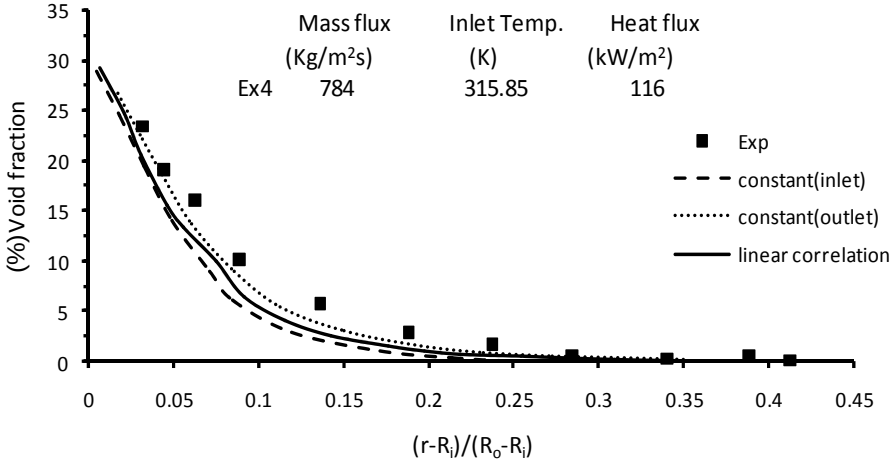

(a)Predicted void fraction profile at M.P.

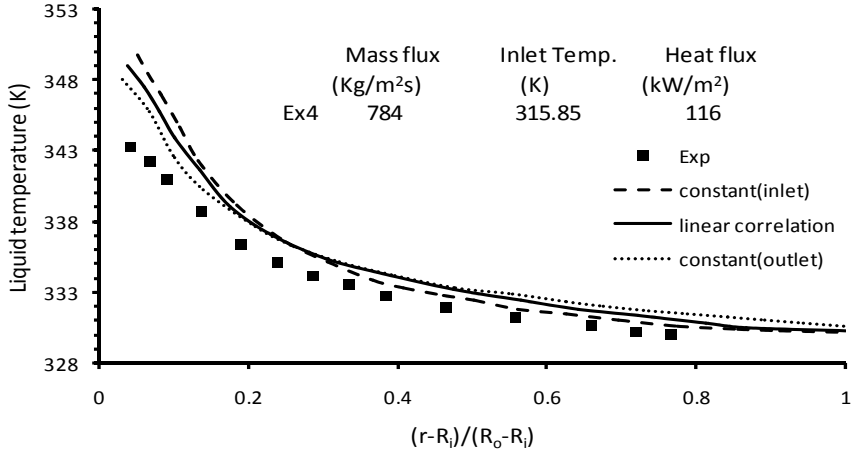

(b) Predicted Liquid temperature profile at M.P.

Figure 4 Influence of saturation temperature.

5.1.3 Influence of non uniform wall heat flux and vapor bubble diameter

In addition to Constant heat flux boundary condition, sinusoidal axial distribution of wall heat flux was adopted on the heated wall. Fig. 5(a)-(c) show the calculated longitudinal and axial distributions of the void fraction and liquid-wall heat transfer coefficient for this case of nonuniform wall heat flux, respectively.

In formulating a two-fluid model for predicting subcooled boiling flow, the local bubble diameter size is one of the important parameters required to estimate the interfacial transfer of mass, momentum and energy [31,32]. Vapor bubbles generated at the heated wall may slide along the wall, eventually depart and travel with the subcooled flow. Meanwhile the vapor bubbles may underlie the process of growth, departure, breakage and coalescence, which is very difficult to model the vapor bubble diameter distribution in the entire flow domain. As measured in the experiment, the probable vapor bubble diameters were between 0.7 mm and 1.3 mm at the measurement plane. When the bubble diameter varies from 0.7 to 1.3 mm, the condensation rate, which is directly proportional to $1/d_b^2$, will decrease and make the liquid temperature lower at the near-wall region. Results indicate that the constant bubble diameter (1.0 mm) is an acceptable simplified method in the present work.

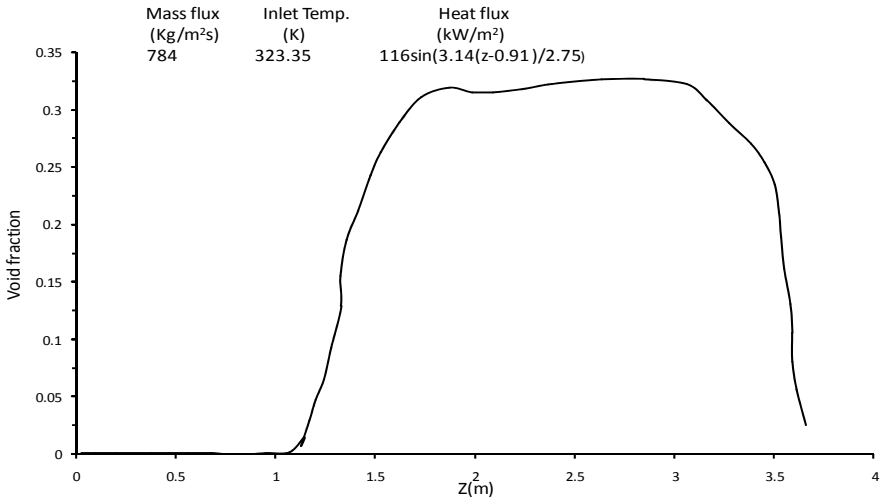

(a) Predicted longitudinal void fraction at heated wall

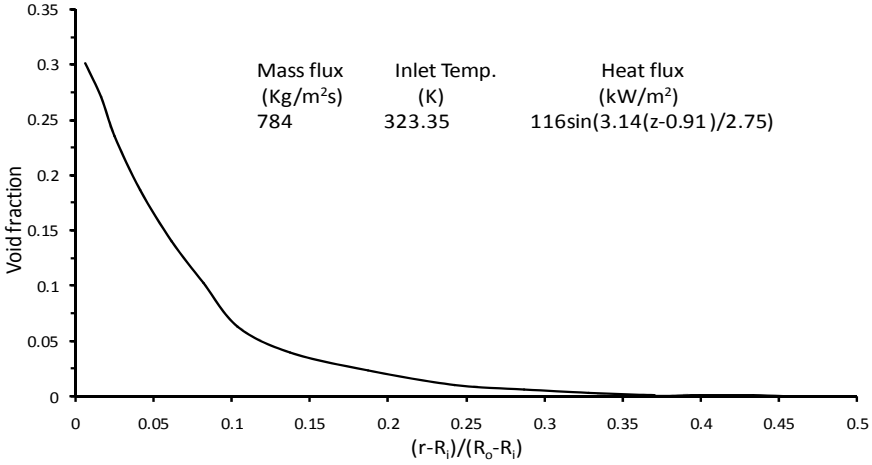

(b) Predicted axial void fraction at M.P.

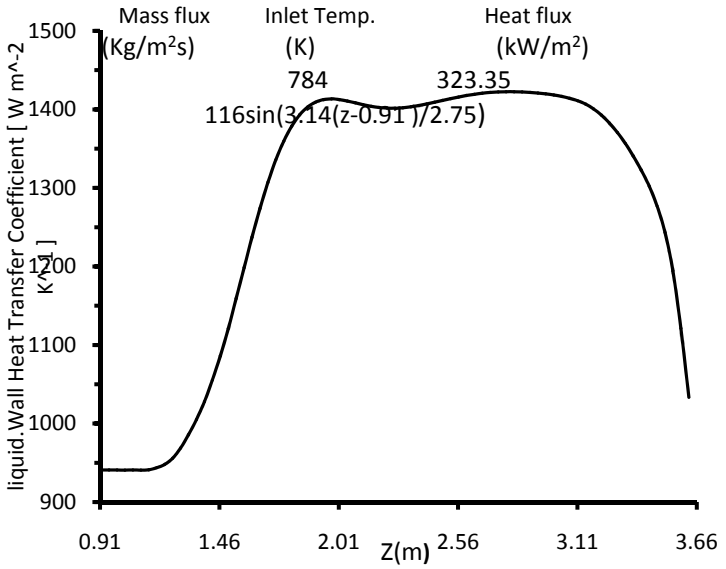

(c) Predicted Liquid-wall heat transfer coefficient along the channel.

Figure 5 Non uniform wall heat flux.

5.2 Void fraction

Fig. 6(a)-(c) presents the radial profile of the predicted and the experimental void fraction at the measurement plane. The local void fraction decreased from the heated wall to the subcooled liquid core, and the region extended by vapor bubbles can be defined as the bubble boundary layer [17]. As shown in Fig. 6, when the wall heat flux increases, the bubble boundary layer will become thicker, and the same results will be also obtained by decreasing the liquid subcooling or the mass flux.

5.3 Liquid-wall heat transfer coefficient

Fig. 7 depicts the liquid-wall heat transfer coefficient along the channel. Predictably, heat transfer coefficient increases by increasing wall heat flux from 95 to 116 (kW/m^2) for the same inlet temperature and mass flux. On the other hand, comparison between cases 2 and 3 reveals that a rise in mass flux leads to an increase in heat transfer coefficient, though there is a reduction in wall heat flux.

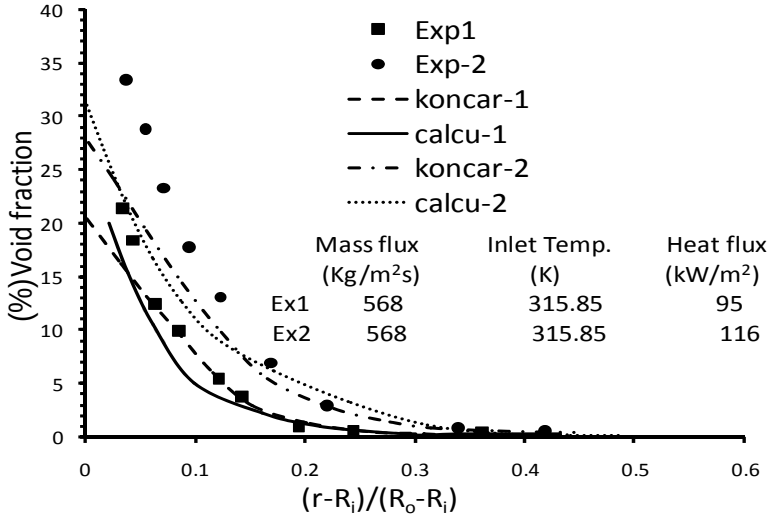

(a)Case 1 and Case 2

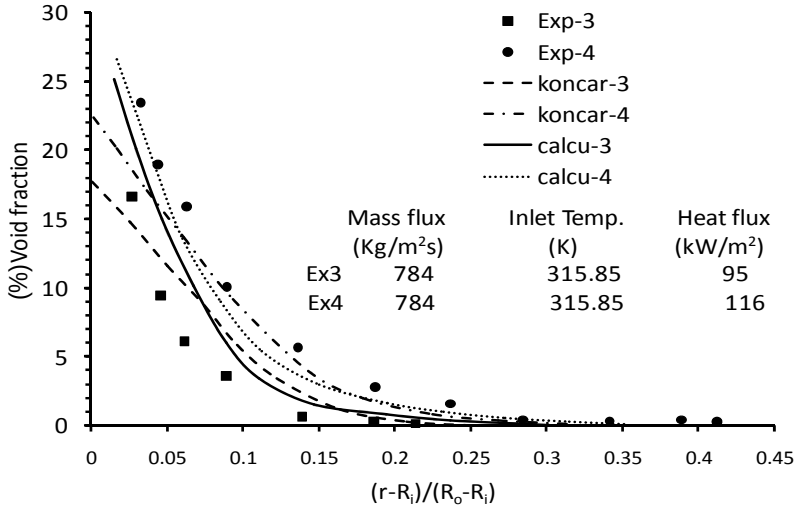

(b) Case 3 and Case 4

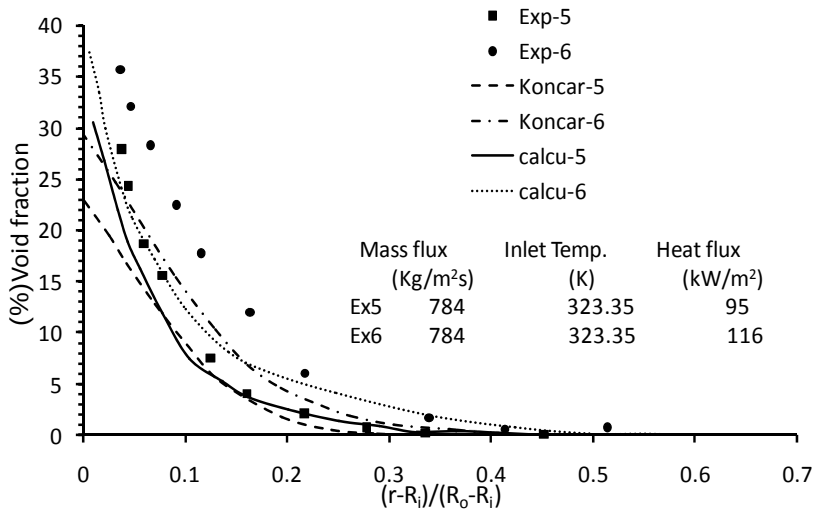

(c)Case 5 and Case 6

Figure 6 Void fraction: predicted and experimental profile at M.P.

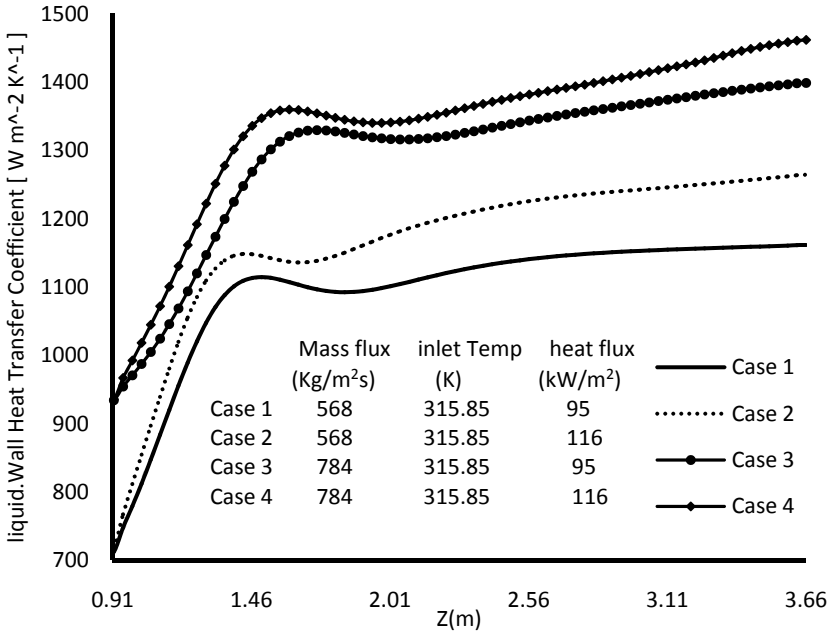

Figure 7 liquid-wall heat transfer coefficient along the channel.

5.4 Liquid temperature

Fig. 8(a)-(c) shows the radial profile of the predicted and the experimental liquid temperature at the measurement plane. As shown in Fig. 8, there is a high temperature gradient at the near-wall region, and the temperature gradient will decrease when approaching to the outer tube. Moreover, as the wall heat flux increases, the predicted and measured liquid temperature profiles become smoother at the near-wall region, which can be interpreted by the increasing turbulent thermal diffusivity in flow region. The turbulent thermal diffusivity has the effect of smoothing the radial liquid temperature profile and can be enhanced by the radial motion of more vapor bubbles with high wall heat flux, which makes the liquid temperature profiles smoother at the near-wall region.

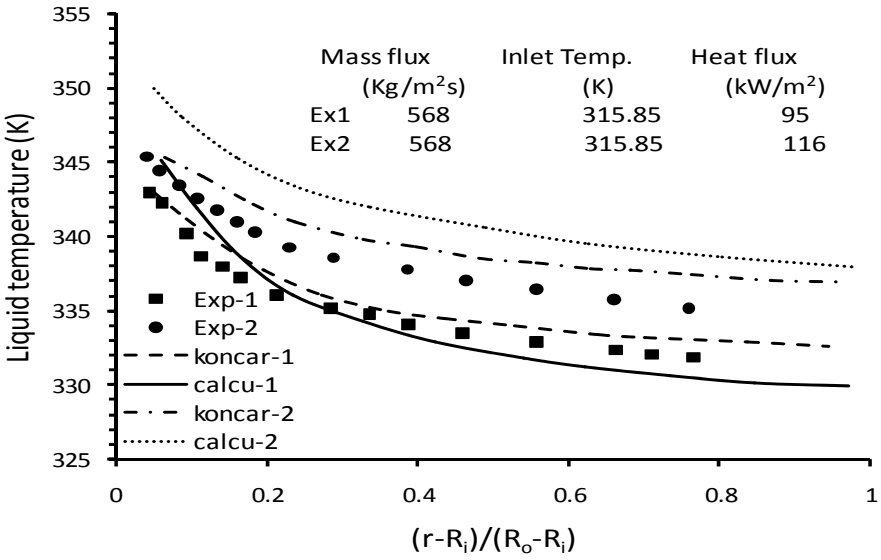

(a) Case 1 and Case 2

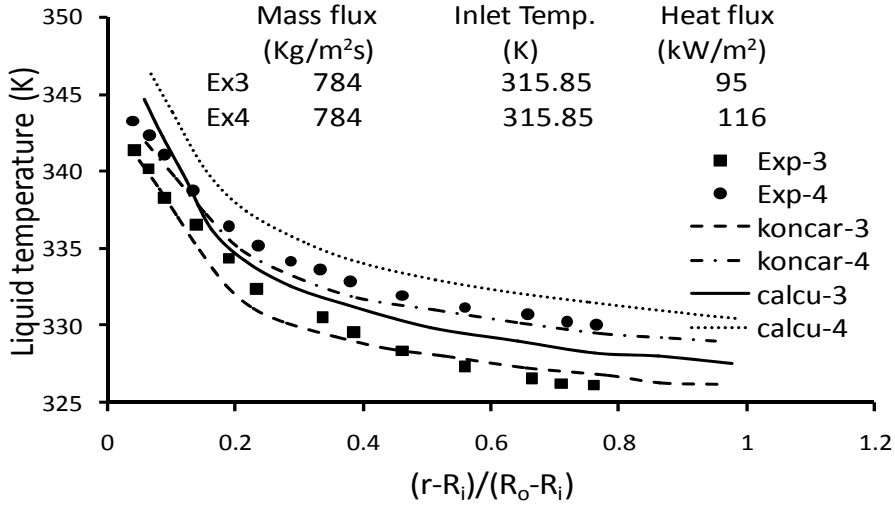

(b) Case 3 and Case 4

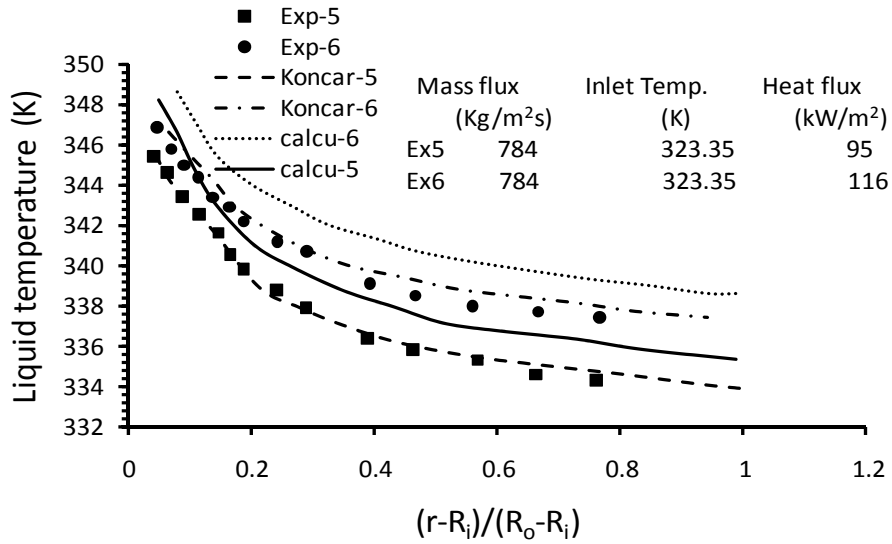

(c)Case 5 and Case 6

Figure 8 Liquid temperature: predicted and experimental profile at M.P.

5.5 Axial liquid and vapor velocity

Figs. 9 and 10(a)-(c) show the radial profile of the predicted and the experimental axial liquid and vapor velocity at the measurement plane, respectively. Compared with the experimental data, large discrepancy occurs at the near-wall region for the axial liquid and vapor velocity profiles in the two predicted results, and the discrepancy will be enhanced with high wall heat flux. As the wall heat flux increases, high void fraction profile will be found in the bubble boundary layer at the measurement plane, which makes the vapor bubbles move faster than the bubbles in lower wall heat flux, and eventually develops the high predicted axial liquid velocity profile with the action of the inter-phase drag force. Especially, the axial liquid velocity in subcooled boiling flow has a peak value near the heated wall, while the axial liquid velocity has a maximum near the center of the channel in single-phase flow. As shown in Fig. 9 (a)-(c), the axial vapor velocity profiles show the similar trend with the axial liquid velocity profiles acted by the inter-phase drag force. The discrepancy of the axial liquid and vapor velocity is mainly caused by the inter-phase momentum transfer, which underlines the need for improvement of dynamic models for momentum transfer.

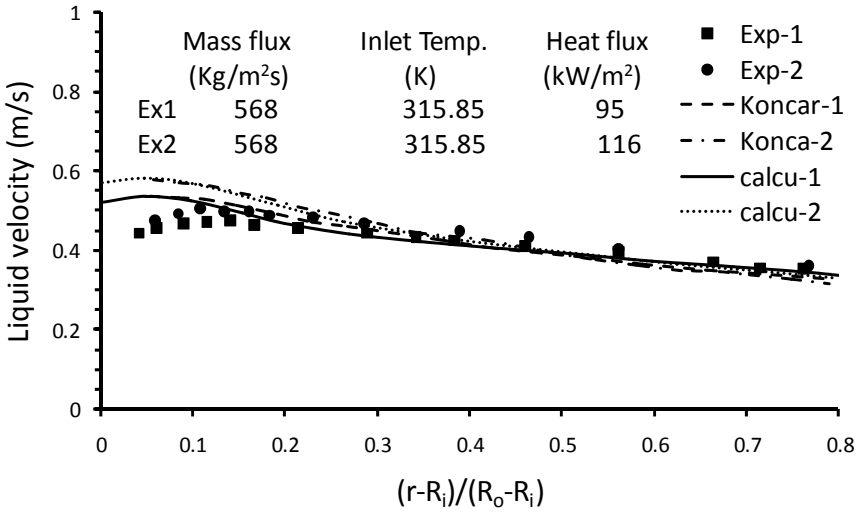

(a)Case 1 and Case 2

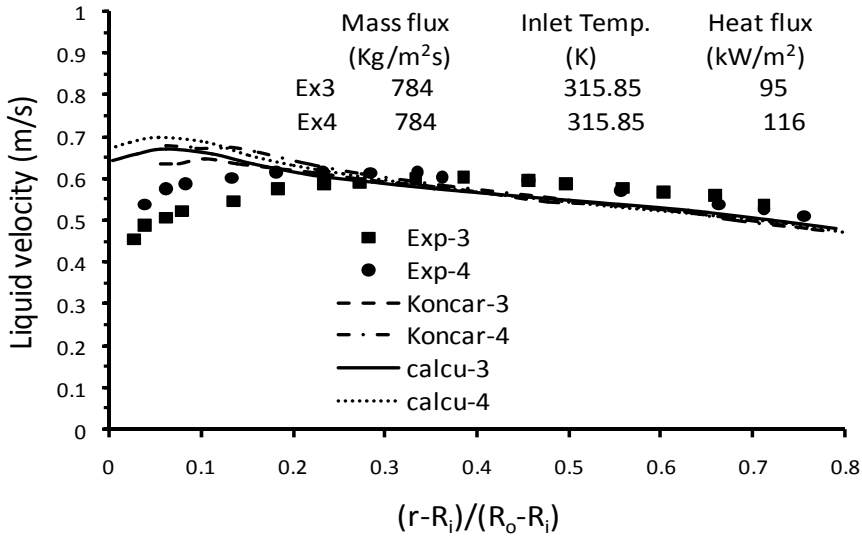

(b) Case 3 and Case 4

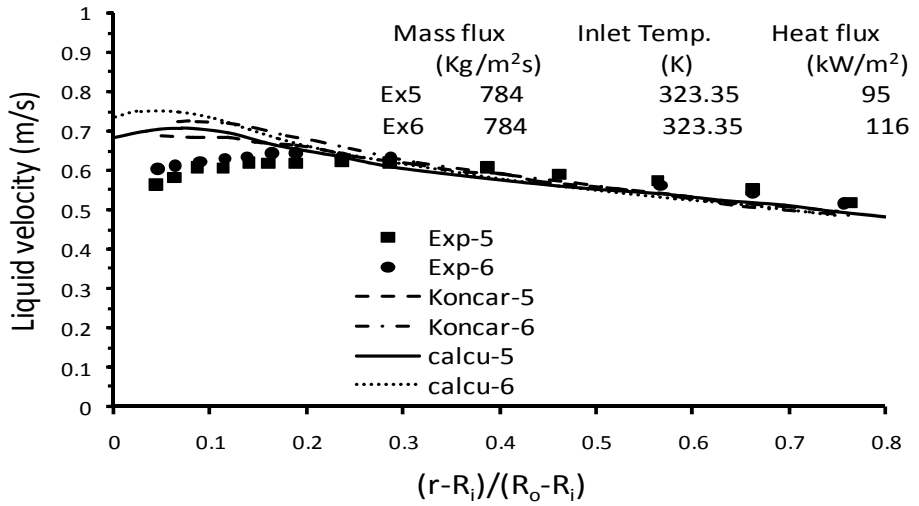

(c) Case 5 and Case 6

Figure 9 Liquid velocity: predicted and experimental profile at M.P.

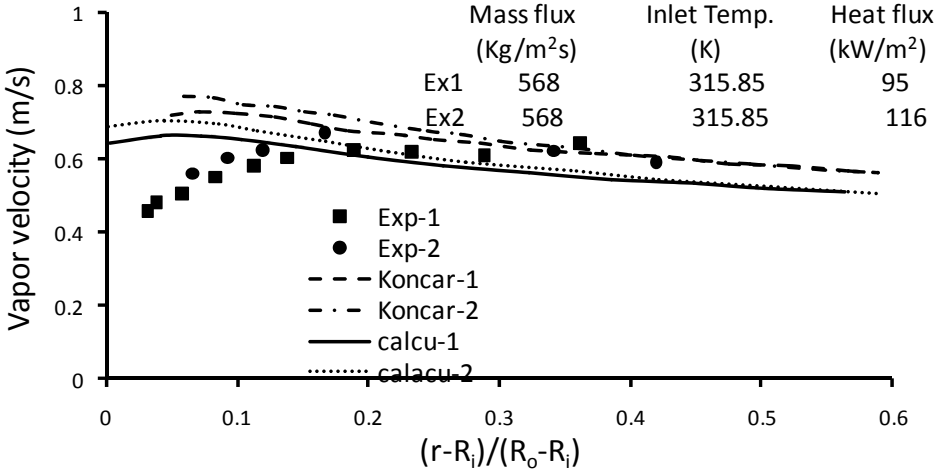

(a) Case 1 and Case 2

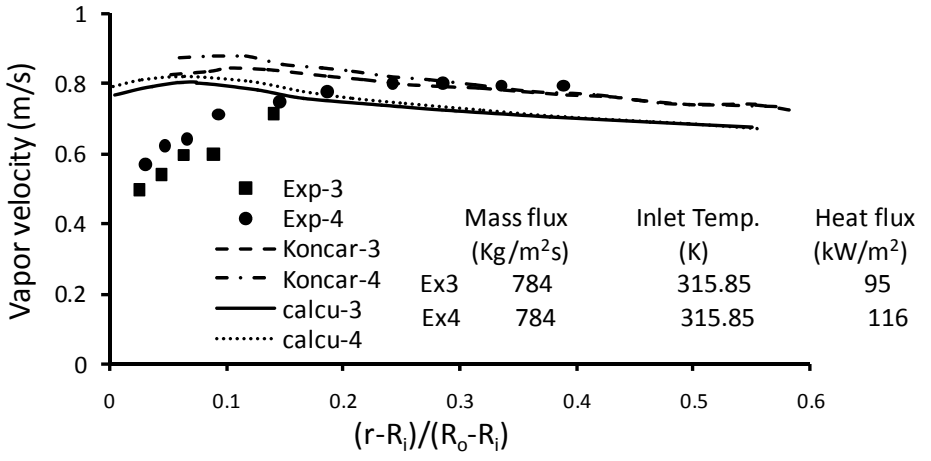

(b) Case 3 and Case 4

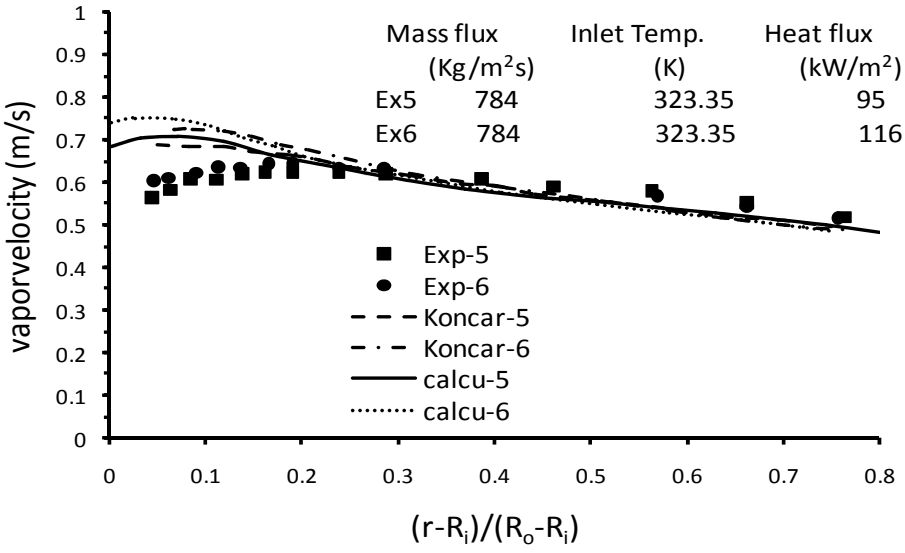

(c) Case 5 and Case 6

Figure 10 Vapor velocity: predicted and experimental profile at M.P.

6 Conclusions

The local flow characteristics of subcooled boiling flow of refrigerant-113 in a vertical concentric annulus have been numerically investigated with a modified two-fluid model, in which temperature dependent properties and saturation temperature variation along the flow direction was considered. The simulation results were validated against the Arizona State University (ASU) boiling flow experiments. Results indicate temperature dependent properties have little influence on the predictions of local flow characteristics in subcooled boiling flow. However, saturation temperature variation along the flow direction is an important factor, which is closely correlative with the predictions of local flow characteristics in subcooled boiling flow. When the saturation temperature adopted is lower than the actual value, higher local void fraction profile and lower liquid temperature profile at the near-wall region will be predicted, and vice versa.

Results show that with increasing the wall heat flux, the bubble boundary layer will become thicker, the liquid temperature gradient at the near-wall region will be smoother and the profiles of axial liquid velocity will gradually depart from those of single-phase flow. Decreasing the liquid subcooling or the mass flux will obtain the same results.

References

[1] Kurul, N., and Podowski, M. Z., "On the Modeling of Multi-dimensional Effects in Boiling Channels," in: 27th National Heat Transfer Conference, Minneapolis, (1991).

[2] Kurul, N., and Podowski, M.Z., "Multidimensional Effects in Forced Convection Subcooled Boiling," in: Proceedings of the Ninth International Heat Transfer Conference, Jerusalem, Israel, pp. 21–26, (1990).

[3] Mimouni, S., Boucker, M., Laviéville, J., Guelfi, A., and Bestion, D., "Modelling and Computation of Cavitation and Boiling Bubbly Flows with the NEPTUNE CFD Code," Nuclear Engineering and Design, Vol. 238, pp. 680–692, (2008).

[4] Krepper, E., Koncar, B., and Egorov, Y., "CFD Modeling of Subcooled Boiling-concept, Validation and Application to Fuel Assembly Design," Nuclear Engineering and Design, Vol. 237, pp. 716–731, (2007).

[5] Lai, J.C., and Farouk, B., "Numerical Simulation of Subcooled Boiling and Heat Transfer in Vertical Ducts," International Journal of Heat and Mass Transfer, Vol. 36, pp. 1541–1551, (1993).

[6] Anglart, H., and Nylund, O., "CFD Application to Prediction of Void Distribution in Two-phase Bubbly Flows in Rod Bundles," Nuclear Engineering and Design, Vol. 163, pp. 81–98, (1996).

[7] Hari, S., and Hassan, Y.A., "Refinement of the RELAP5/MOD3.2 Subcooled Boiling Model for Low-pressure Conditions," In: Proceedings of the 8th International Conference ICONE-8, Baltimore, MD, USA, (2000).

[8] Koncar, B., Kljenak, I., and Mavko, B., "Modelling of Local Two-phase Flow Parameters in Upward Subcooled Flow Boiling at Low Pressure" International Journal of Heat and Mass Transfer, Vol. 47, pp. 1499–1513, (2004).

[9] Hainoun, A., Hicken, E., and Wolters, J., "Modeling of Void Formation in the Subcooled Boiling Regime in the ATHLET Code to Simulate Flow Instability for Research Reactors," Nuclear Engineering and Design, Vol. 167, pp. 175–191, (1996).

[10] Janssens-Maenhout, G., Knebel, J.U., and Mueller, U., "Subcooled Nucleate Boiling at Low Pressure and Low Heat Flux," in: Proceedings of 3rd International Conference on Multiphase Flow, Lyon, France, (1998).

[11] Lee, T.H., Park, G.C., and Lee, D.J., "Local Flow Characteristics of Subcooled Boiling Flow of Water in a Vertical Concentric Annulus," International Journal of Multiphase Flow, Vol. 28, pp. 1351–1368, (2002).

[12] Legendre, D., Boree, J., and Magnaudet, J., "Thermal and Dynamic Evolution of a Spherical Bubble Moving Steadily in a Superheated or Subcooled Liquid," Physics of Fluids, Vol. 10, pp. 1256–1272, (1998).

[13] Kljenak, I., Park, G.C., Mavko, B., and Lee, T., "Bubble-tracking Modeling of Subcooled Nucleate Boiling in a Vertical Annulus," in: Proceedings of the 12th International Heat Transfer Conference, Grenoble, France, pp. 767–772, (2002).

[14] Stpierre, C.C., and Bankoff, S.G., "Vapor Volume Profiles in Developing Two-phase Flow," International Journal of Heat and Mass Transfer, Vol. 10, pp. 237–249, (1967).

[15] Sekoguchi, K., Tanaka, O., Esaki, S., Katsuki, N., and Nakasatomi, M., "Prediction Method of Flow Patterns in Subcooled and Low Quality Boiling Regions," Bulletin of the Japan Society of Mechanical Engineers. Eng, Vol. 24, pp. 834–841, (1981).

[16] Bartel, M.D., "Experimental Investigation of Subcooled Boiling," M.Ss. Thesis in Nuclear Engineering, Purdue University, West Lafayette, IN, USA, (1999).

[17] Chen, E., Li, Y., and Cheng, X., "CFD Simulation of Upward Subcooled Boiling Flow of Refrigerant-113 using the Two-fluid Model," Applied Thermal Engineering, Vol. 29, pp. 2508–2517, (2009).

[18] Ishii, M., and Mishima, K., ''Two-fluid Model and Hydrodynamic Constitutive Relations,'' Nuclear Engineering and Design, Vol. 82, pp. 107–126, (1984).

[19] ANSYS-CFX Development Team, "Solver Theory, Multiphase Flow Theory," CFX-12 Documentation, ANSYS, (2009).

[20] Lemmert, M., and Chawla, J.M., "Influence of Flow Velocity on Surface Boiling Heat Transfer Coefficient," in: E. Hahne, U. Grigull (Eds.), *Heat Transfer in Boiling*, Academic Press and Hemisphere, (1977).

[21] Ivey, H.J., "Relationships Between Bubble Frequency, Departure Diameter and Rise Velocity in Nucleate Boiling," International Journal of Heat and Mass Transfer, Vol. 10, pp. 1023–1040, (1967).

[22] Tolubinski, V. I., and Kostanchuk, D. M., "Vapour Bubbles Growth Rate and Heat Transfer Intensity at Subcooled Water Boiling", 4th International Heat Transfer Conference, Paris, France, (1970).

[23] Ranz, W. E., and Marshall, W. R., ''Evaporation from Drops,'' Chemical Engineering Progress, Vol. 48, pp. 142–180, (1952).

[24] Ishii, M., and Zuber, N., "Drag Coefficient and Relative Velocity in Bubbly, Droplet or Particulate Flows", AIChE (The American Institute of Chemical Engineering) Journal, Vol. 25, pp. 843-855, (1979).

[25] Tomiyama, A., "Struggle with Computational Bubble Dynamics", 3rd International Conference on Multiphase Flow, Lyon, France, pp. 1-18, (1998).

[26] Antal, S. P., Lahey, R. T., and Flaherty, J. E., "Analysis of Phase Distribution in Fully Developed Laminar Bubbly Two-phase Flow", International Journal of Multiphase Flow, Vol. 7, pp. 635-652, (1991).

[27] Rhie, C.M. and Chow, W.L., "A Numerical Study of the Turbulent Flow Past an Isolated Airfoil with Trailing Edge Separation", AIAA J., pp. 82-0998, (1982).

[28] Kang, S., and Roy, R.P., "Vapor Phase Measurements in Subcooled Boiling Flow," Journal of Heat Transfer, Vol. 124, pp. 1207–1209, (2002).

[29] Koncar, B., and Krepper, E., "CFD Simulation of Convective Flow Boiling of Refrigerant in a Vertical Annulus," Nuclear Engineering and Design, Vol. 238, pp. 693–706, (2008).

[30] Sato, Y., Sadatomi, M., and Sekoguchi, K., "Momentum and Heat Transfer in Two-phase Bubble Flow," International Journal of Multiphase Flow, Vol. 7, pp. 167–177, (1981).

[31] Lucas, D., Krepper, E., and Prasser, H.M., "Prediction of Radial Gas Profiles in Vertical Pipe Flow on Basis of the Bubble Size Distribution," International Journal of Thermal Science, Vol. 40, pp. 217–225, (2001).

[32] Bartel, M.D., Ishii, M., Masukawa, T., Mi, Y., and Situ, R., "Interfacial Area Measurements in Subcooled Flow Boiling," Nuclear Engineering and Design, Vol. 210, pp. 135–155, (2001).

Nomenclature

a_i	Interfacial area density (m^{-1})
A_{bub}	Nucleating bubbles area fraction
C_D	Drag coefficient for bubbles
C_L	Lift force coefficient
C_P	Specific heat ($J.Kg^{-1}.K^{-1}$)
C_{TD}	Turbulent dispersion force coefficient
d_b	Bubble diameter (m)
d_{bw}	Bubble departure diameter (m)
Eo	Eotvos number
F_D	Drag force ($Kg.m.s^{-2}$)
F_L	Lift force ($Kg.m.s^{-2}$)
F_{TD}	Turbulent dispersion force ($Kg.m.s^{-2}$)
F_W	Wall lubrication force ($Kg.m.s^{-2}$)
f	Bubble nucleation frecuency (s^{-1})
g	Gravitational acceleration ($m.s^{-2}$)
H	Enthalpy ($J.Kg^{-1}$)
h_i	Inter-phase heat transfer coefficient ($W.m^{-2}.K^{-1}$)
H_{lg}	Latent heat ($J.Kg^{-1}$)
N_a	Active nucleation sites density
Nu	Nusselt number
p	Pressure ($N.m^{-2}$)
Pr	Prandtel number
q_c	Single-phase convective heat flux ($W.m^{-2}$)
q_e	Evaporating heat flux ($W.m^{-2}$)
q_Q	Quenching heat flux ($W.m^{-2}$)
q_w	Wall heat flux ($W.m^{-2}$)
r	Interfacial volume density
Re	Reynolds number
S_t	Stanton number
T	Temperature (K)
u	Velocity ($m.s^{-1}$)

Greek symbols

α	Phase fraction
β	Thermal expansion coefficient (K^{-1})
Γ	Phase change rate ($Kg.m^{-3}.s^{-1}$)

μ Total dynamic viscosity (Pa.s)
ρ Density (Kg.m^{-3})
σ Surfase tension (N.m^{-1})
σ_t Turbulent schmit umber
τ Shear stress (N.m^{-1})
τ_Q Quenching period (s)
λ Thermal conductivity (W.m^{-1}.K^{-1})

Subscripts

e Evaporation
g Vapor phase
i Interphase
l Liquid phase
s Saturated
w Wall

چکیده

در مطالعه حاضر از مدل توسعه یافته دو سیالی برای شبیه سازی پدیده جوشش همرفتی سیال R-113 در یک کانال حلقوی عمودی در فشار پایین استفاده شده است. در این مدل توسعه یافته، اثرات وابستگی خصوصیات سیال به دما و نیز تغییرات دمای اشباع در طول کانال لحاظ شده و نتایج بدست آمده با تعدادی از مطالعات آزمایشگاهی و عددی منتشر شده ارزیابی شده است. نتایج پژوهش حاضر در مطابقت خوبی با نتایج تجربی شامل پروفیل های شعاعی کسر حجمی بخار، سرعت های هر دو فاز و دمای فاز مایع میباشد. علاوه بر شار حرارتی یکنواخت، شار حرارتی سینوسی نیز به دیواره کانال اعمال گردیده است. نتایج نشان می دهد که با افزایش شار حرارتی، لایه مرزی حباب ضخیم تر شده و پروفیل های سرعت محوری فاز مایع در این حالت به تدریج از پروفیل های آن برای جریان تک فازی فاصله میگیرد.